J. Mol. Biol. (1991) **221**, 47–53

Comparison of the Solution Nuclear Magnetic Resonance and X-ray Crystal Structures of Human Recombinant Interleukin-1β

G. Marius Clore and Angela M. Gronenborn

Laboratory of Chemical Physics, Building 2
National Institute of Diabetes and Digestive and Kidney Diseases
National Institutes of Health
Bethesda, MD 20892, U.S.A.

(Received 5 April 1991; accepted 10 May 1991)

The solution structure of interleukin-1β determined by nuclear magnetic resonance spectroscopy is compared to three independently solved X-ray structures at 2 Å resolution. It is shown that the solution and X-ray structures are very similar, both locally and globally. The atomic root-mean-square (r.m.s.) difference between the solution and X-ray structures is ~0·9 Å for backbone atoms, ~1·5 Å for all atoms and ~1 Å for all atoms of internal residues. The largest differences are confined to some of the loops and turns connecting β-strands. The atomic r.m.s. distribution of the 32 calculated solution structures about their mean co-ordinate positions (~0·4 Å for backbone atoms, ~0·8 Å for all atoms and ~0·5 Å for all atoms of internal residues) is approximately the same as the atomic r.m.s. differences between the three X-ray structures, indicating that the positional errors in the atomic co-ordinates determined by the two methods are similar.

Keywords: interleukin-1β; solution structure; X-ray structure; nuclear magnetic resonance

Interleukin-1β (IL-1β†) is a member of the cytokine family of proteins and plays a key role in the immune and inflammatory responses (Dinarello, 1989). We recently presented the determination of its high resolution structure in solution by three-dimensional (3D) and four-dimensional (4D) heteronuclear nuclear magnetic resonance (n.m.r.) spectroscopy (Clore *et al.*, 1991; Brookhaven Protein Data Bank accession codes 6I1B and 7I1B). At 153 residues, IL-1β is 50% larger in terms of number of residues than any other n.m.r. protein structure published to date (Dyson *et al.*, 1990; Forman-Kay *et al.*, 1991), and represents the first example of the successful application of multi-dimensional heteronuclear n.m.r. methods to structure determination of proteins in the 15 to 20,000 Da range. While the n.m.r. study was underway, two X-ray structures at 2 Å (1 Å = 0·1 nm) resolution were published (Finzel *et al.*, 1989; Priestle *et al.*, 1989; Protein Data Bank accession codes 1I1B and 2I1B, respectively) and the co-ordinates of a third X-ray structure have recently also been deposited in the Brookhaven Protein Data Bank (Veerpandian *et al.*, 1991; Protein Data Bank accession code 4I1B). Here, we present a comparison of the solution and X-ray structures of IL-1β.

The solution structure of IL-1β is based on a total of 3146 experimental restraints comprising 2630 interproton distance restraints, 114 distance restraints for 57 hydrogen bonds associated with slowly exchanging NH protons, 36 distance restraints relating to hydrogen bonds involving seven bound water molecules, and 366 torsion angle restraints involving 152 ϕ, 115ψ and 99 χ_1 angles. The three X-ray structures were obtained from the *same* crystal form (space group $P4_3$ and, within experimental error, identical unit cell dimensions) and have been solved at the *same* resolution (2 Å) to a comparable degree of refinement (*R*-factor ≤19%). Statistical aspects of the comparison between the n.m.r. and X-ray structures are summarized in Tables 1 to 3 and Figure 4, and various best-fit superpositions are shown in Figures 1 to 3. As described previously, the structure of IL-1β is made up of 12 β-strands arranged in three pseudo-symmetric topological units, each of which comprises five strands (Figs 1 and 2).

The best-fit superpositions of the backbone atoms of the whole molecule (residues 3 to 151) and of the three repeating topological units and their interface, shown in Figures 1 and 2, respectively, clearly illustrate that the n.m.r. and X-ray structures are very

† Abbreviations used: IL-1β, interleukin-1β; 3D, three-dimensional; 4D, four-dimensional; n.m.r., nuclear magnetic resonance; r.m.s., root-mean-square.

0022-2836/91/170047-07 $03.00/0

Table 1

Comparison of Lennard–Jones van der Waals' energy, solvation free energy of folding and covalent geometry for the n.m.r. and X-ray structures of IL-1β

Structure	E_{L-J}† kcal mol^{-1}	SFE† kcal mol^{-1}	Deviations from idealized covalent geometry‡		
			Bonds (Å)	Angles (°)	Impropers (°)
⟨SA⟩	−570±11	−183±2·5	0·005±0	1·868±0·002	0·523±0·006
(SA)r	−561	−189	0·005	2·109	0·556
X-ray-1	−539	−184	0·029	5·288	2·794
X-ray-2	−538	−184	0·019	4·789	1·337
X-ray-3	−512	−185	0·025	4·621	6·125

The notation of the structures is as follows: ⟨SA⟩ are the final 32 simulated annealing structures obtained from the n.m.r. data (Protein Data Bank code 7I1B); SA is the mean structure obtained by averaging the co-ordinates of the individual simulated annealing structures best fitted to each other (excluding residues 1, 152 and 153); (SA)r is the restrained minimized mean structure obtained from SA (code 6I1B). The n.m.r. structures were calculated using the hybrid distance geometry–dynamical simulated annealing method of Nilges *et al.* (1988). X-ray-1, X-ray-2 and X-ray-3 are the X-ray structures of Finzel *et al.* (1989: code 1I1B), Priestle *et al.* (1989: code 2I1B) and Veerapandian *et al.* (1991: code 4I1B), respectively.

† E_{L-J} is the Lennard–Jones van der Waals' energy calculated using the CHARMM (Brooks *et al.*, 1983) empirical energy function. SFE is the solvation free energy of folding calculated as described by Eisenberg & McLachlan (1986).

‡ The larger deviations in bond angles and improper torsions (which refer to planes and chirality) for the X-ray structures relative to those for the n.m.r. structures reflect the nature of the target function employed. Specifically, these terms are described indirectly by distance restraints in the case of the crystallographic least-squares refinement programs, PROLSQ (Hendrickson & Konnert, 1980) and RESTRAIN (Haneef *et al.*, 1985), used in the X-ray structure determinations, whereas these terms are described directly by angles in the case of the simulated annealing program XPLOR (Brünger *et al.*, 1986; Brünger, 1990) used for the n.m.r. structure determination. Direct angular restraints are more restrictive than the indirect distance restraints, as very small deviations in these distances can result in quite large deviations in angles.

similar both globally and locally. This is particularly evident not only for the backbone atoms in the regions of regular secondary structure (Fig. 2), but also for the side-chains of internal residues (Fig. 3). In addition, the overall quality of the n.m.r. and X-ray structures, as judged by the small deviations from idealized covalent geometry, and the large negative values of the Lennard–Jones van

Table 2

Atomic r.m.s. differences between the n.m.r. and X-ray structures of IL-1β

	Atomic r.m.s. difference (Å)					
	Residues 3–151†			Internal residues‡		
	Backbone atoms	All atoms	All atoms excluding ambiguities§	Backbone atoms	All atoms	All atoms excluding ambiguities§
A. *n.m.r.* versus *X-ray*						
⟨SA⟩ *versus* X-ray-1	0·94±0·06	1·51±0·05	1·28±0·05	0·72±0·04	1·01±0·05	0·89±0·04
⟨SA⟩ *versus* X-ray-2	0·97±0·06	1·66±0·05	1·41±0·05	0·72±0·04	1·06±0·05	0·94±0·04
⟨SA⟩ *versus* X-ray-3	0·96±0·06	1·62±0·05	1·38±0·05	0·74±0·04	1·09±0·05	0·98±0·03
(SA)r *versus* X-ray-1	0·85	1·33	1·13	0·68	0·92	0·81
(SA)r *versus* X-ray-2	0·88	1·54	1·30	0·67	0·99	0·87
(SA)r *versus* X-ray-3	0·87	1·47	1·26	0·70	1·01	0·91
B. *X-ray* versus *X-ray*						
X-ray-1 *versus* X-ray-2	0·39	1·02	0·79	0·15	0·54	0·49
X-ray-1 *versus* X-ray-3	0·25	0·72	0·61	0·22	0·54	0·49
X-ray-2 *versus* X-ray-3	0·43	1·09	0·86	0·24	0·62	0·55
C. *n.m.r.*						
⟨SA⟩ *versus* SA	0·40±0·04	0·81±0·04	0·66±0·04	0·28±0·03	0·49±0·03	0·40±0·03
(SA)r *versus* SA	0·13	0·39	0·26	0·09	0·25	0·16
⟨SA⟩ *versus* (SA)r	0·42±0·04	0·90±0·04	0·71±0·04	0·29±0·03	0·55±0·04	0·43±0·03

The notation of the structures is the same as that in Table 1. The r.m.s. differences involving all atoms refer to heavy atoms (i.e. C, N, O, S) and exlude protons.

† As residues 1, 152 and 153 are partially disordered in the n.m.r. structure, and residues 1 to 2 are not visible in the electron density maps of the X-ray structures, the comparison is restricted to residues 3 to 151.

‡ Internal residues are defined by a surface accessibility in the structure of ≤40% than that of the corresponding residue in an extended Gly-X-Gly tripeptide (Chothia, 1976).

§ These comparisons exclude the $O^{\delta 1}$ and $O^{\delta 2}$ atoms of Asp, the $O^{\delta 1}$ and $N^{\delta 2}$ atoms of Asn, the $O^{\varepsilon 1}$ and $O^{\varepsilon 2}$ atoms of Glu, the $O^{\varepsilon 1}$ and $N^{\varepsilon 2}$ atoms of Gln and the $N^{\eta 1}$ and $N^{\eta 2}$ atoms of Arg, as the identities of these atoms are ambiguous in the X-ray structures.

Table 3

Comparison of agreement of X-ray structures with the experimental n.m.r. interproton distance and torsion angle restraints

	Violations 0·5–1·0 Å/1·0–2·0 Å/>2·0 Å		
	X-ray-1	X-ray-2	X-ray-3
A. *Interproton distance restraints*†			
Interresidue			
Sequential ($\|i-j\|=1$) (592)	11/1/0	24/ 1/0	11/3/0
Short ($1<\|i-j\|\leq 5$) (265)	9/0/0	10/10/3	12/6/1
Long ($\|i-j\|>5$) (848)	17/3/0	18/14/2	24/9/9
Intraresidue (925)	3/1/0	8/ 4/0	5/3/0
	Violations >40°		
	X-ray-1	X-ray-2	X-ray-3
B. *Torsion angle restraints*‡			
ϕ	0	6	0
ψ	0	2	0
χ_1 internal residues§	0	2	4
χ_1 surface residues§	2	15	3

The complete set of experimental n.m.r. restraints are deposited in the Brookhaven Protein Data Bank with the code name R6I1BNMR. The interproton distance restraints are classified into 3 ranges, 1·8 to 2·7 Å, 1·8 to 3·3 Å (1·8 to 3·5 Å for nuclear Overhauser effects involving NH protons), and 1·8 to 5·0 Å corresponding to strong, medium and weak nuclear Overhauser effects, respectively. The minimum ranges employed for ϕ, ψ and χ_1 torsion angle restraints are $\pm 30°$, $\pm 50°$ and $\pm 20°$, respectively. The notation of the structures is the same as that in Table 1.

† The total number of interproton distance restraints in each category is given in parentheses.

‡ The torsion angle restraints comprise 152 ϕ, 115 ψ and 99 χ_1 torsion angles.

§ Internal and surface residues are defined by a surface accessibility of $\leq 40\%$ and $>40\%$ of the same residue in an extended Gly-X-Gly tripeptide segment (Chothia, 1976).

der Waals' energy and solvation free energy of folding (Eisenberg & McLachlan, 1986), is comparable (Table 1). Interestingly, the latter is $\sim 20\%$ more negative than the predicted value for a protein of this size (Clichet *et al.*, 1990) and can be attributed to a densely packed hydrophobic core (see Fig. 3).

From the data in Table 2, it is apparent that the errors in the atomic co-ordinates of the X-ray and n.m.r. structures are similar, as judged by the fact that the atomic root-mean-square (r.m.s.) differences between the X-ray structures are approximately the same as those of the 32 individual n.m.r. structures about their mean co-ordinate positions. This is true not only of the backbone atoms but also for all atoms, and perhaps more importantly for all atoms of internal residues. These errors, and particularly those for all atoms, even when restricted to ordered internal residues, are significantly larger than the value of 0·22 to 0·23 Å (Finzel *et al.*, 1989; Veerpandian *et al.*, 1991) obtained from a Luzzati (1952) plot of *R*-factor *versus* resolution. This leads one to conclude that, in this particular case at least, the Luzzati error analysis underestimates the positional errors in X-ray atomic co-ordinates, with the exception of those for the backbone atoms of internal residues.

Despite the overall similarities, there are some discernible differences between the structures. This is shown by the observation that the atomic r.m.s. differences between the n.m.r. and X-ray structures are larger than either the atomic r.m.s. distribution of the individual n.m.r. structures about their mean co-ordinate positions or the atomic r.m.s. differences between the three X-ray structures (Table 2 and Fig. 4). (Note that the simulated annealing protocol employed in the n.m.r. structure determination samples fully the conformational space consistent with the experimental n.m.r. data (Nilges *et al.*, 1988).) Further support for this notion can be drawn from the fact that the X-ray structures display violations for several interproton distance and torsion angle restraints derived from the n.m.r. data that lie outside experimental error (Table 3). The majority of these violations are different for the three X-ray structures. Thus, there are no interproton distance violations >2 Å in common between the three X-ray structures. In the case of interproton distance violations in the 1 to 2 Å range, there is one sequential restraint common to all three X-ray structures (Val3($C^{\beta}H$)-Arg4(NH)), three short-range interresidue restraints common to X-ray structures 2 and 3 (Asp86($C^{\beta 2}H$)-Tyr90($C^{\epsilon}H$), Ser125($C^{\beta 1}H$)-Met130($C^{\beta 1}H$) and Thr137($C^{\gamma}H$)-Gln141($N^{\epsilon 2}H$)), two long-range interresidue

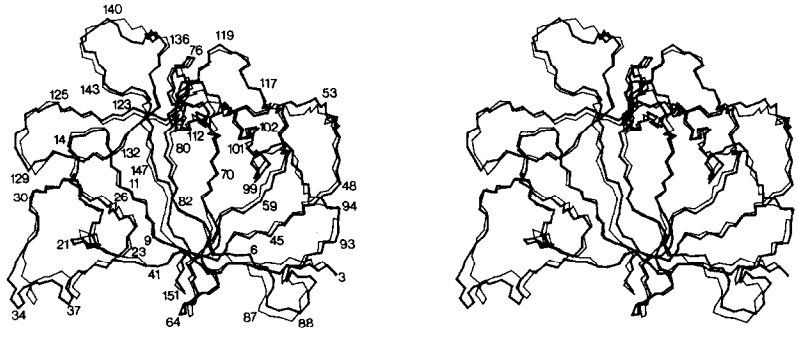

Figure 1. Best-fit superposition of the backbone (N, C^{α} and C) atoms of the restrained minimized mean n.m.r. (thick lines) and X-ray (thin lines) structures of IL-1β for residues 3 to 151. The X-ray structure is that of Finzel *et al.*, 1989.

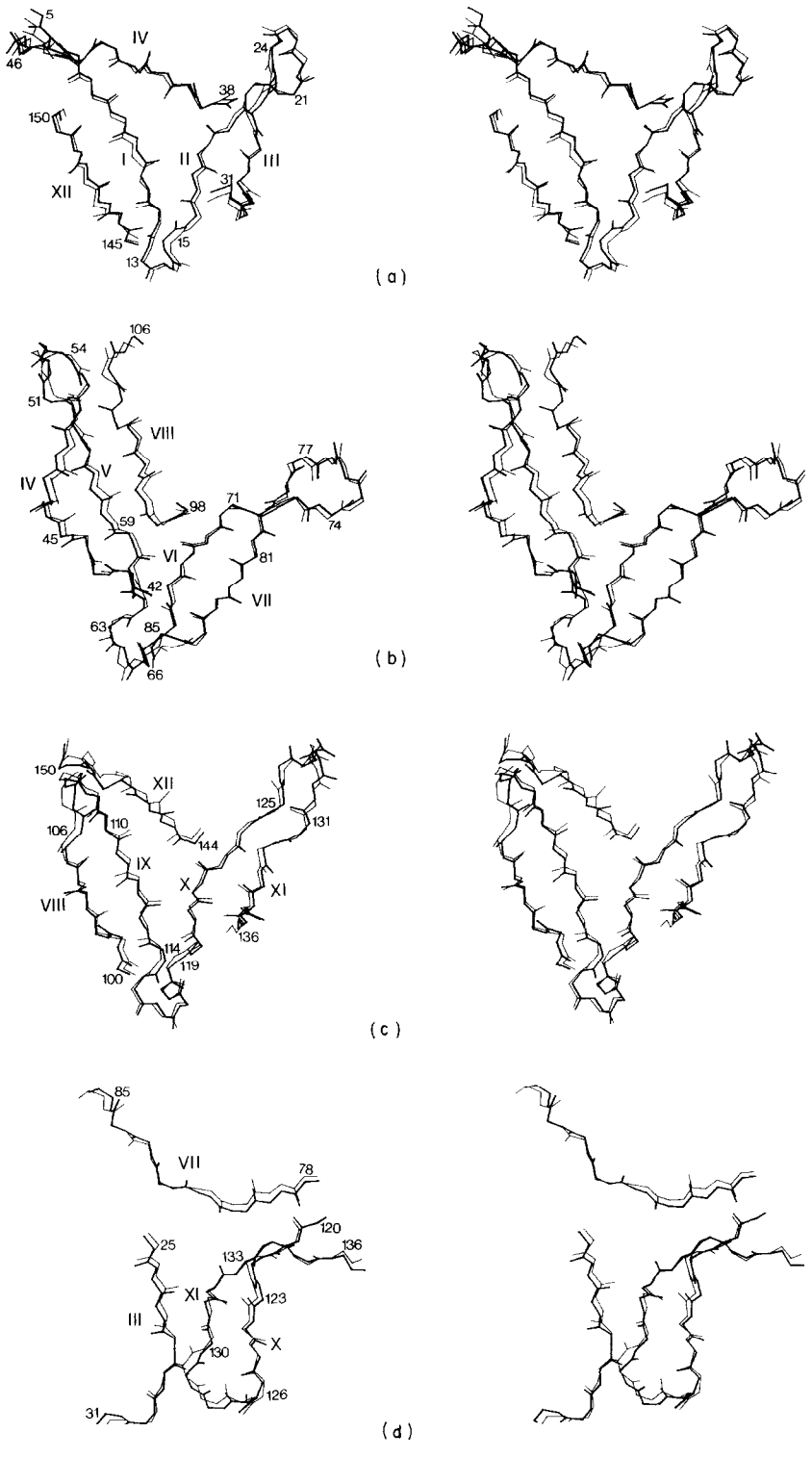

Figure 2. Best-fit superposition of the backbone (N, C^{α}, C and O) atoms of the restrained minimized mean n.m.r. (thick lines) and X-ray (thin lines) structures of IL-1β for the 3 repeating topological units of IL-1β (a) to (c) and the interface of 3 units (d). Each topological unit is composed of 5 anti-parallel β-strands. The X-ray structure is that of Finzel *et al.* (1989).

restraints common to X-ray structures 2 and 3 (Glu25(NH)-Leu82($C^{\delta 1}$H) and Glu25(C^{α}H)-Leu82($C^{\delta 1}$H)), one intraresidue restraint common to X-ray structures 1 and 3 (Lys97(NH)-Lys97(C^{δ}H)), and one intraresidue restraint common to X-ray structures 2 and 3 (Leu82(NH)-Leu82(C^{γ}H)). Violations in ϕ and ψ torsion angles are only seen for X-ray structure 2 and involve surface exposed residues in turns or loops. All the χ_1 torsion angle violations arise from different rotamers relative to that specified by the n.m.r. restraint. Again, there are no cases in which the same χ_1 torsion angle

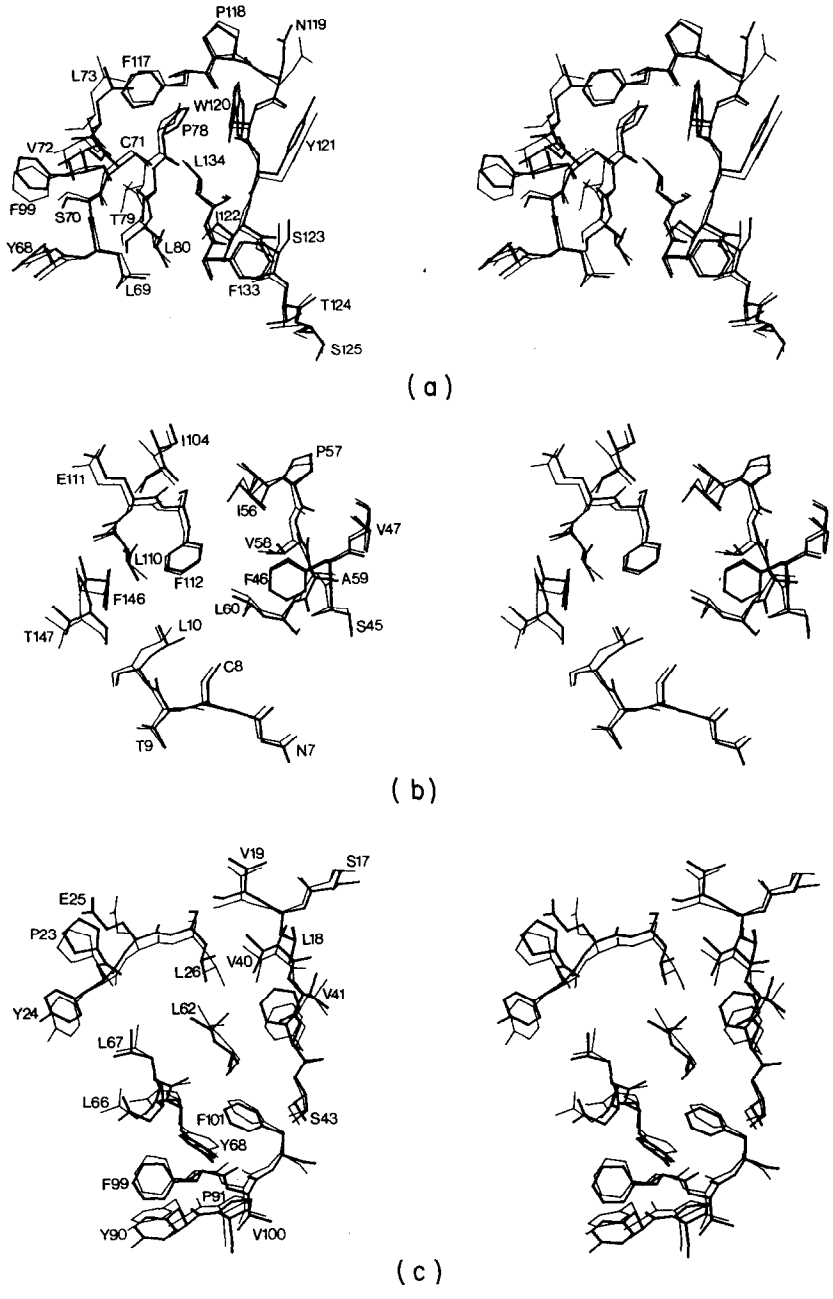

Figure 3. Best-fit superposition of all atoms (excluding protons) of the restrained minimized mean n.m.r. (thick lines) and X-ray (thin lines) structures for 3 selected segments of IL-1β. The X-ray structure is that of Finzel *et al.* (1989).

violation involves all three X-ray structures, and only three cases where the same χ_1 torsion angle violation involves two of the three X-ray structures. The latter comprise χ_1 for Gln14, Gln15 and Ser125 in X-ray structures 2 and 3; Gln14 and Gln15 are surface residues, whereas Ser125 is an internal residue.

The main structural differences between the X-ray and n.m.r. structures are confined to five loops and turns which serve to link β-strands. The first involves a small rigid body displacement (i.e. a hinge-like motion) of the 3_{10} helix (residues 32 to 39) that connects strands III and IV, such that the C^{α}–C^{α} distance between residue 34 and residue 150 in strand XII (see bottom left of the structure in Fig. 1) is reduced from 20·5 Å in the n.m.r. structure to 17·9 Å in the X-ray structure. Two other small rigid body displacements are seen for the 84 to 91 loop connecting strands VII and VIII (bottom right of Fig. 1) and the 106 to 109 turn connecting strands VIII and IX (Fig. 2(c)). In all three cases these involve small concerted changes in ϕ and/or ψ torsion angles in the outer residues comprising the linker regions. In the case of the turn (residues 52 to 55) connecting strands IV and V (Fig. 1, top right) and the loop (residues 136 to 142) connecting strands XI and XII (Fig. 1, top left), on the other hand, the differences are localized to two neighboring residues (Asn53 and Asn54, Gly139 and Gly140, respectively). In assessing the significance

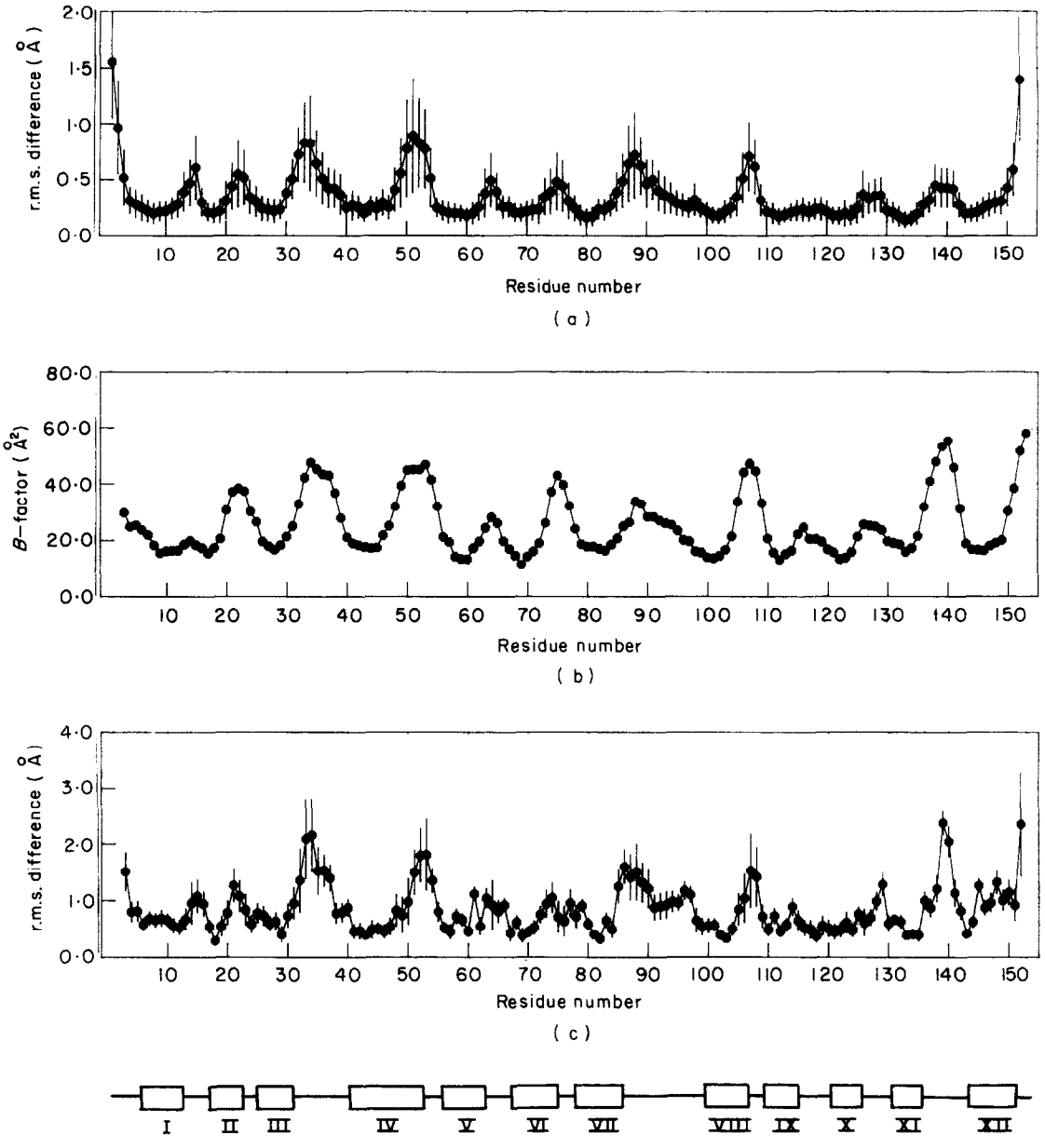

Figure 4. Comparison of (a) the backbone atomic r.m.s. distribution of the 32 simulated annealing n.m.r. structures about their mean co-ordinate positions, (b) the crystallographic *B*-factors for the backbone atoms from the X-ray structure, and (c) the backbone atomic r.m.s. difference between the 32 simulated annealing structures and the X-ray structure. The X-ray structure is that of Finzel *et al.* (1989). In the case of (a) and (c) the filled circles represent the average values at each residue and the bars the standard deviations of these values. The location of the 12 β-strands is indicated below the Fig.

of these structural differences, it is worth noting that residues 32 to 39 and 84 to 91 are involved in contacts with adjacent molecules in the crystal lattice that could account for the observed displacements. The other regions are associated with the largest *B*-factors in the X-ray structure and the largest atomic r.m.s. distributions about the mean co-ordinate positions in the n.m.r. structures (Fig. 4), and hence comprise the least well defined regions in both sets of structures.

The *B*-factors of the backbone atoms of the X-ray structure display an approximately sinusoidal variation along the polypeptide chain (Fig. 4) with ten regions, principally located in the turns and loops connecting the β-strands, having unusually high *B*-factors (Finzel *et al.*, 1989). The *B*-factors provide a measure of mean-square displacements of the atoms in the crystal and are related to both static and dynamic disorder. It is interesting to note that there is an almost perfect correlation between the backbone variation in the atomic r.m.s. distribution of the n.m.r. structures, the *B*-factors and the atomic r.m.s. differences between the n.m.r. and X-ray structures (Fig. 4). The variations in atomic r.m.s. distribution observed for the n.m.r. structures provide a measure of the precision of the atomic positions of the solution structure, which, in turn, are determined by the density of short interproton

distance contacts (<5 Å) at any particular location in the molecule. For exposed turns and loops, the density of short interproton distance contacts is naturally reduced, so that the precision with which their atomic positions can be determined by n.m.r. is decreased. Indirectly, this may be related to motion, as a smaller number of short interproton distance restraints implies a reduction in non-bonded contacts, and hence packing restrictions, which one would expect to be accompanied by increased atomic mobility. A direct measure of backbone mobility, both with respect to amplitude and time scales, can only be obtained by heteronuclear ^{15}N or ^{13}C relaxation measurements. Such measurements have been carried out on IL-1β (Clore *et al.*, 1990). These studies reveal that the large atomic r.m.s. differences and *B*-factors observed in the turns or loops connecting strands II and III, III and IV, IV and V, VII and VIII, VIII and IX, and X and XI, involve residues which exhibit atomic motions on the 0·5 to 4 nanoseconds time scale, while those in the segments connecting strands V and VI, and XI and XII are correlated with motions on a time scale of 30 nanoseconds to 10 milliseconds associated with ^{15}N T_2 line broadening.

In summary, the present study reveals that the solution structure of IL-1β as determined by n.m.r. and three independently solved X-ray crystal structures are very similar in terms of both global and local features. The atomic r.m.s. distribution observed for the 32 calculated n.m.r. structures is of the same order of magnitude as that between the three X-ray structures, indicating that the errors in the atomic co-ordinates for structures determined by the two methods are comparable.

This work was supported by the AIDS Targeted Anti-Viral Program of the Office of the Director of the National Institutes of Health.

References

Brooks, B. R., Bruccoleri, R. E., Olafson, B. D., States, D. J., Swaminathan, S. & Karplus, M. (1983). CHARMM: a program for macromolecular energy minimization and dynamics calculations. *J. Comput. Chem.* **4**, 187–217.

Brünger, A. T. (1990). *XPLOR Version 2.1 Manual*, Yale University Press, New Haven, CT.

Brünger, A. T., Clore, G. M., Gronenborn, A. M. & Karplus, M. (1986). Three dimensional structures of proteins determined by molecular dynamics with interproton distance restraints: application to crambin. *Proc. Nat. Acad. Sci., U.S.A.* **83**, 3801–3805.

Chothia, C. (1976). The nature of the accessible and buried surfaces in proteins. *J. Mol. Biol.* **105**, 1–14.

Clichet, L., Gregoret, L. M., Cohen, F. E. & Kollman, P. A. (1990). Protein model structure evaluation using the solvation free energy of folding. *Proc. Nat. Acad. Sci., U.S.A.* **87**, 3240–3243.

Clore, G. M., Driscoll, P. C., Wingfield, P. T. & Gronenborn, A. M. (1990). Analysis of backbone dynamics of interleukin-1β using two-dimensional inverse detected heteronuclear 15N-1H NMR spectroscopy. *Biochemistry*, **29**, 7387–7401.

Clore, G. M., Wingfield, P. T. & Gronenborn, A. M. (1991). High-resolution three-dimensional structure of interleukin-1β in solution by three- and four-dimensional nuclear magnetic resonance spectroscopy. *Biochemistry*, **30**, 2315–2323.

Dinarello, C. A. (1989). Review of the biology of interleukin-1. *Advan. Immunol.* **44**, 153–205.

Dyson, H. J., Gippert, G. P., Case, D. A., Holmgren, A. & Wright, P. E. (1990). Three-dimensional solution structure of the reduced form of *Escherichia coli* thioredoxin determined by nuclear magnetic resonance spectroscopy. *Biochemistry*, **29**, 4129–4136.

Eisenberg, D. & McLaghlan, A. D. (1986). Solvation energy in protein folding and binding. *Nature (London)*, **319**, 199–203.

Finzel, B. C., Clancy, L. L., Holland, D. R., Muchmore, S. W., Watenpaugh, K. D. & Einspahr, H. M. (1989). Crystal structure of recombinant human interleukin-1β at 2·0 Å resolution. *J. Mol. Biol.* **209**, 779–791.

Forman-Kay, J. D., Clore, G. M., Wingfield, P. T. & Gronenborn, A. M. (1991). The high resolution three-dimensional structure of reduced recombinant human thioredoxin in solution. *Biochemistry*, **30**, 2685–2698.

Haneef, I., Moss, D. S., Stanford, M. J. & Borkakoti, N. (1985). RESTRAIN: conventional restrained least-squares refinement program. *Acta Crystallogr. sect. A*, **41**, 426–433.

Hendrickson, W. A. & Konnert, J. H. (1980). Incorporation of stereochemical information into crystallographic refinement. In *Computing in Crystallography* (Diamond, R., Ramaseshan, S. & Venkatesan, K., eds), pp. 13.01–13.23, Indian Institute of Science, Bangalore.

Luzzati, V. (1952). Treatment of statistical errors in the determination of crystal structures. *Acta Crystallogr.* **5**, 802–810.

Nilges, M., Clore, G. M. & Gronenborn, A. M. (1988). Determination of three dimensional structures of proteins from interproton distance data by hybrid distance geometry-dynamical simulated annealing calculations. *FEBS Letters*, **229**, 317–324.

Priestle, J. P., Schär, H. P. & Grütter, M. G. (1989). Crystallographic refinement of interleukin-1β at 2·0 Å resolution. *Proc. Nat. Acad. Sci., U.S.A.* **86**, 9667–9671.

Veerapandian, B., Gilliland, G. L., Raag, R., Svensson, A. L., Masui, Y., Hirai, Y. & Poulos, T. L. (1991). Functional implications of interleukin-1β based on the three dimensional structure. *Prot. Struct. Funct. Genet.* In the press.

Edited by P. E. Wright